

$ee\in MC$: Low Energy Mesons and the Residual QCD Potential

Ian M. Nugent*
Victoria, B.C., Canada

Abstract

The Flux-Tube Breaking Model in $ee\in MC$ is expanded to include the residual QCD potential between the Final-State mesons, within the non-relativistic limit. These residual QCD potentials have been predicted in the context of the Flux-Tube Breaking Models to generate meson-meson molecular states for the $f_0(500)$, $f_0(980)$, $a_0(980)$, through the colour hyper-fine spin-spin interaction. These residual potentials are also found to have an important impact on the S_1 decay of the a_1 and K_1 axial-vector mesons due to the colour hyper-fine spin-spin interaction. It is found that in the low mass regions, the $\rho(770)$ and $K^*(892)$ are sensitive to the linear-confining potential and colour-Coulomb potential suggesting that with the high statistics at the B-Factories, it may be possible to probe the linear-confining potential and colour-Coulomb potential through a model dependent description of the resonance shape or by exploiting multiple production process.

Keywords: Electron-Positron Collider, Tau Lepton, Monte-Carlo Simulation

1 Introduction

Inter-meson interactions through the residual QCD potential have been proposed in the Flux-Tube-Breaking models as an explanation for the low energy $f_0(500)$, $f_0(980)$, $a_0(980)$, and $K_0^*(700)$ scalar states [1, 2, 3, 4, 5]. Within this picture, the residual QCD potential in the Final-State forms inter-meson “molecular” states [1, 2, 3]. This interpretation is supported by evidence from ψ and $\eta(1440)$ decays in $\pi\pi - KK$ scattering and scalar $\gamma\gamma$ coupling couplings [3, 6, 7, 8]. The production of the scalar mesons through this mechanism does not depend on the chiral symmetry and is therefore an alternative hypothesis to models in which the low mass scalar mesons are directly related to the origin of the quark-composite mass through chiral symmetry breaking [9, 10, 11, 12, 13, 14, 15, 16, 17, 18, 19, 20, 21, 22, 23, 24, 25]. This provides a complementary alternative hypothesis for the low mass scalars to [26]. These wave-function amplitude distortions from Final-State residual QCD meson interactions are not only limited to the S-wave channel, but are predicted to play an essential role in low energy “meson-evolution” [5]. Within the context of the Flux-Tube Breaking Model [27, 28, 29, 30], supplemented with phenomenological models of the residual QCD potential, we extend the models to the majority of decays of light quark mesons within the Flux-Tube Breaking Model presented in [26].

2 Low Energy QCD Potential Models

The residual QCD interaction between the outgoing Final-State mesons modifies the cross-section (decay-rate) through both corrections to the meson propagators and

wave-function amplitude distortion [1, 2, 3]. At low energies the modification to the hadronic propagators are expected to be negligible [3], and will therefore be neglected in this work. This leaves the wave-function amplitude distortions caused by the Final-State interaction between the mesons,

$$S_{h_1 h_2}^2 = \frac{\sigma(h_0 \rightarrow h_1 h_2 | V(r))}{\sigma(h_0 \rightarrow h_1 h_2)} \approx \frac{|\psi(r=0 | V(r))|^2}{|\psi(r=0)|^2}. \quad (1)$$

It follows from equation 1, that in the Flux-Tube Breaking Model, the width of the meson resonances is also dependant on $S_{h_1 h_2}^2$, and therefore must be included in the computation of the mass dependent width $\Gamma(s)$, and the effective mass of the resonances, \hat{m}^2 and \bar{m}^2 . These amplitude distortions to the wave-function from the effective QCD potential on the outgoing wave-function of the Final-State hadrons can be approximated by the non-relativistic relative Hamiltonian for plane waves being scattered by a potential in the non-relativistic static limit [3]. Although, the validity of this approximation can be questioned in the relativistic regime [3], the predominate effect is in the low energy non-relativistic region. In the relativistic regime, $S_{h_1 h_2}$ converges to unity. Within this context, the radial component of the wave-function, $\psi(r, \theta, \phi) = R(r) Y_m^l(\theta, \phi)$, is determined numerically [31, 32] from the Schrödinger equations in spherical coordinates,

$$R''(r) = -\frac{2}{r} R'(r) + 2\mu \left(\frac{l(l+1)}{2\mu r^2} + V(r) - E_{h_1 h_2} \right) R(r) \quad (2)$$

where l is the angular momentum and μ is the reduced mass of the system. The initial conditions correspond to the Spherical Bessel Functions $J_0(x)$, $J_1(x)$ and $J_2(x)$ for the S-wave, P-wave and D-wave respectively [33] at the origin of production for the Final-State particles ($r=0/x=0$).

*Corresponding Author

Email: inugent.physics@outlook.com

From the Flux-Tube Breaking Model, the largest contribution to the potential energy for the light quark mesons produced in a S-wave state is due to the colour hyperfine spin-spin interaction [34]. This is described in the Flux-Tube Breaking Model by the expectation value of the Hamiltonian. For a single meson this may be written as:

$$\langle \psi_{nS} | H_{hyp} | \psi_{nS} \rangle = \frac{32 \hat{S}_i \cdot \hat{S}_j \pi \alpha_s}{9 m_i m_j} |\psi_{nS}(0)|^2 \quad (3)$$

[27, 34] where $\alpha_s=0.6$ [35] is the frozen coupling constant, \hat{S}_i and \hat{S}_j are the spin operators for the i th and j th valence quark from the Initial-State meson. m_i and m_j correspond to the mass of the i th and j th valence quark in the non-relativistic static potential, $m_{u/d}=0.22GeV/c^2$ and $m_s=0.419GeV/c^2$ [35]. For two mesons $\beta_B=\beta_C=\beta$ in a ground state emitted in a S_1 configuration, this reduces

$$V_{hyp}(r) = \frac{32 \alpha_s \hat{S}_i \cdot \hat{S}_j \beta^3}{9(2\pi)^{1/2} m_i m_j} e^{-\frac{(\beta r)^2}{2}} \quad (4)$$

by means of convolution of the two Gaussians [36]. For the P and D-wave production, the expectation value of the colour hyperfine spin-spin interaction is not expected to contribute based-on the orthogonality of states and symmetry [37]. For the K_1 system, the expectation value of the spin-spin operator, $\hat{S}_i \cdot \hat{S}_j$, is not the same between the singlet and triplet states, and therefore must be incorporated into the mixing of the singlet and triplet states [26, 38, 39, 40]. Thus the potential for the colour hyper-fine spin-spin interaction may not only be attractive but also repulsive in the S_1 decays of the $K_1(1270)$ and $K_1(1400)$ mesons depending on the given s . For the case were $\beta_B \neq \beta_C$, the colour hyper-fine spin-spin potential may be written as:

$$V_{hyp}(r) = \frac{32 \alpha_s \hat{S}_i \cdot \hat{S}_j (\beta_B^3 \beta_C + \beta_B \beta_C^3)}{18(\pi)^{1/2} (\beta_B^2 + \beta_C^2)^{1/2} m_i m_j} e^{-\frac{(\beta_B \beta_C r)^2}{(\beta_B^2 + \beta_C^2)}} \quad (5)$$

where symmetrization between the wave-functions has been applied for the respective normalizations¹.

The remaining potentials in the Flux-Tube Breaking Model, are due to the linear-confining potential,

$$V_L^{I=0} = -\frac{C_7^2 b}{3\pi} \left(\beta r + 2\sqrt{\frac{2}{\pi}} - \left(\beta r + \frac{2}{\beta r} \right) \text{Erf} \left(\frac{\beta r}{2} \right) \right) e^{-\frac{(\beta r)^2}{2}} - \frac{2}{\sqrt{\pi}} e^{-\frac{3(\beta r)^2}{4}} \quad (6)$$

[34] and colour-Coulomb potential,

$$V_C^{I=0}(r) = \frac{4C_7^2 \alpha_s}{9r} \left(1 + \sqrt{\frac{2}{\pi}} \beta r - 4 \text{Erf} \left(\frac{\beta r}{2} \right) \right) e^{-\frac{(\beta r)^2}{2}} \quad (7)$$

[34]². From the symmetrization of the transition matrix it follows that $V_C^{I=0} = -V_C^{I=1}$ and $V_L^{I=0} = -V_L^{I=1}$ [34]³.

¹In the results presented here $\beta_B=\beta_C=0.4$, only β_A in the axial-vector mesons deviates from $\beta=0.4$ in this work with a value of $\beta=0.35$.

²We note that the $f_0(1370)$ and $K_0^*(1430)$ are 3P_0 states and that the wave-function overlap is approximated as resulting from S wave particles.

³We follow the $I=1$ and $I=0$ sign convention from [34].

From Figure 1, it can be seen, that there is a potential for bound states to be formed for the S-wave production, which is qualitatively consistent with [3]. Naïvely, one would expect that the bound states would be below the $h_1 h_2$ production threshold and would decay either electromagnetically or weakly, while other models predict higher mass pseudo-stable bound meson-meson molecular states [41]⁴. The bound states are not investigated in this paper, but instead, we will focus on the scattering of the hadronic plane waves in the continuum which cause the Final-State interaction between the hadrons.

In addition to the Flux-Tube Breaking potentials, we include phenomenological models to investigate the theoretical sensitivity to the core-meson potential and residual external potential. The colour hyper-fine spin-spin interaction potential associated with this Final-State interaction between the mesons is modeled as a sum of the short-range residual QCD potential for each meson. Based on imperial evidence [3], and the latter Flux-Tube Breaking Model description, it is modelled using a Gaussian for the S-wave production channels which is normalized to the values extracted in [3]. For consistency with the Flux-Tube Breaking potentials [3], $r_0=a_0/\sqrt{2}$ with a_0 representing the charge radius of the meson. This is combined with an effective potential for the colour-Coulomb potential outside of the mesons and the core potential inside the mesons based on the shell model [42]. In these models, the phenomenological functional form approximates the colour-Coulomb potential for a given colour charge density distributed and is therefore finite⁵. These models include a parabolic distribution based on the Shell Model [42] with no external residual QCD potential (Parabolic), a parabolic core distribution with a Yukawa residual QCD potential (Parabolic-Yukawa) and the Woods-Saxon potential for the Shell Model [42, 43]. The normalization is obtained from the linear-confining and colour-Coulomb terms in the Flux-Tube Breaking Model at $r=\beta(r=a_0)$. The definition for each of these potentials and the corresponding parameters can be found in Tables 1 and 2. This gives effective potentials of $\mathcal{O}(10 - 100MeV)$ which are consistent with nuclear potentials in the Shell Model [42].

3 Modification to the Flux-Tube Breaking Model

The Flux-Tube Breaking Model [27, 28, 29, 30, 35] implemented in **eeMC** [26] is extended to include an enhanced vector decay-width calculation which incorporates higher threshold decay processes while the $f_0(1370)$ decay processes are extended to include the $\gamma\gamma$ channel. This is achieved by replacing the formalism for the f_{VPP} form-factor from [30, Eq. A.16], with the formalism in [27]⁶.

⁴If the stable bound meson-meson molecular states have a sufficiently long life-time, they could be a potential background for dark-matter searches.

⁵The colour charge density goes to 0 within the meson surface layer which has a mean value of the charge radius[42].

⁶This includes applying the corresponding corrections throughout the program.

This is particularly important for the $\rho(770)\rightarrow KK$ contribution which has an amplitude/A of $\frac{\sqrt{3}}{2}P_1$. The non-strange low energy scalar sector in the Flux-Tube Breaking Model [26], in particular, the $f_0(500)$ and $f_0(980)$, is described in terms of a threshold effect from $\pi^0\pi^0$, $\pi^+\pi^-$, K^+K^- and $K^0\bar{K}^0$ for the $f_0(1370)$ meson resulting from the dispersion relation [26]. These threshold effects are sensitive to lower mass threshold decay processes. As such, the threshold effects from the $\pi^0\pi^0$ and $\pi^+\pi^-$ are expected to be extremely sensitive to the $\gamma\gamma$ channel which has thus far not been included. Therefore the $f_0(1370)$ model is extended to incorporate the $f_0(1370)\rightarrow\gamma\gamma$ contribution determined within the Bethe-Salpeter bound state formalism [44] where the scalar amplitude $A({}^3P_0=0^{++})$ is approximated by means of the Flux-Tube-Breaking Model [35]. The decay width may be written as:

$$\Gamma(s) = \frac{S|M|^2}{16\pi M_{f_0(1370)}} = \frac{|F_S(s) \sum_i \sum_j \epsilon^{\alpha\beta\gamma\delta} \epsilon_{(i)\alpha}^* q_{\beta} \epsilon_{(j)\gamma}^* q_{\delta}'|^2}{16\pi M_{f_0(1370)}} \quad (8)$$

where

$$F_S(s) = \frac{\sqrt{24\pi}\alpha_{QED}(s)e_Q^2 A({}^3P_0)}{M_{f_0(1370)}^{3/2} m_Q^2}. \quad (9)$$

The running of $\alpha_s(s)$ in the scalar amplitude $A({}^3P_0=0^{++})$ is taken into account using an effective phenomenological model of a saturated coupling in the low mass region [35, Fig. 2]. The inclusion of the $f_0(1370)\rightarrow\gamma\gamma$ decay channel suppresses the $\pi^0\pi^0$ and $\pi^+\pi^-$ threshold effects, as seen in Figure 2. This can be seen in both the purely time-orders propagator and the propagator with non-resonant contributions,

$$P(s) = \frac{\alpha}{s-\tilde{m}^2(s)+im_0\Gamma(s)} + \frac{1-\alpha}{2m_0(\sqrt{s-\tilde{m}(s)}+im_0\Gamma(s))} \quad (10)$$

[26]. The resulting $f_0(1370)\rightarrow\gamma\gamma$ decay width is $\Gamma(s)=2.4MeV$ which is comparable to the width extracted from Belle data Mushkelishvili-Omnés method (2.1keV)[45, 46, 47] and consistent with other predictions [45, Fig. 40]. For mesons composed of relativistic light quarks, the contribution from the binding energy, $E_B=m-m_Q$, is non-negligible⁷. The static limit for the decay width [44] is taken as an alternative to estimate the impact of the binding energy in the light-quark systems. From Figure 2, it can be seen that in the static limit, the low mass region in the $f_0(1370)$ propagator is significantly enhanced.

4 Impact of the Low Energy QCD Potential

Figures 3 and 5 show a comparison of the simulated 2-hadron and 3-hadron decay spectra for the Flux-Tube

⁷ m_Q is the quark mass determined for a simple-harmonic oscillator wave-function within an approximate QCD potential which includes an exchange term + linear-confining and corrections for relativistic effects [35].

Breaking Model with the wave-function amplitude distortions applied along with Chiral-Resonance-Lagrangian (ChRL) Models and Vector Dominance Models for comparison. The impact of the wave-function amplitude distortions on the $f_0(1370)$ propagator line-shape is illustrated in Figure 2 for each of the decay channels. Only the $\pi\pi$ channels show the double peak structure that was predicted in [26]. The large enhancement in the KK channels explains why the measured $f_0(980)$ primarily decays through the KK channels relative to the $\pi\pi$ channels. In [4], it was shown that the $q\bar{q}q\bar{q}$ composition of the $f_0(980)$ and $a_0(980)$ may be formed through a mixture of meson-states which is due to the amplitude of strong annihilation processes. In this case the meson composition of the effective potentials must be constructed from a super-positioning of the meson potential. This would be manifested through the relative KK and $\pi\pi$ branching fractions of the $f_0(1370)$ and $a_0(980)$ mesons, as observed in [3, 6, 7, 8]⁸. When interpreting the predictions, it is important to note which regions are relativistic and which are non-relativistic. The threshold regions which have the largest wave-function amplitude distortions are non-relativistic. When the particle becomes relativistic, the wave-function amplitude distortions tend to unity. Near the $\rho(770)$ peak and the $a_1(1260)$ peak for the $\rho(770)\pi$ channel, the outgoing mesons are relativistic. The $K^*(892)K$ contribution to the $a_1(1260)$ is non-relativistic. The outgoing mesons near the $K^*(892)$ and $\rho(770)$ peaks in the decays of the K_1 mesons are only quasi-non-relativistic with a $\beta\approx 0.5$. From Figure 3, it can be seen that the P-wave $\tau^-\rightarrow\rho(700)\rightarrow\pi^-\pi^0\nu_\tau$ production for the Flux-Tube Breaking Model relative to the Gounaris-Sakurai Model [48, 49] in [26] are consistent depending on the fraction of purely time-ordered contribution to the propagator. From Figure 1, the model dependence is sufficient for some discrimination between the model with the high statistics expected at Belle-II, however, this sensitivity may be limited by the knowledge of the fraction of purely time-ordered resonant contribution to the propagator, as seen in Figures 3 and 4 near the $\pi^-\pi^0$ threshold. Detailed studies are required to determine if the shape information can separate these two effects in individual decay processes. In Figure 5, for the $a_1(1260)$ and K_1 mesons, the wave-function amplitude distortion is primarily due to the colour hyper-fine spin-spin interaction in the S_1 production and therefore has a significant impact on the S/D-wave ratio near threshold of the vector and pseudo-scalar mesons, particularly for the K_1 mesons. This has to be taken into account in any extraction of the mixing angle, θ_{K_1} , and or the $SU(3)_f$ Flavour Breaking Factor δ_{K_1} [26, 38, 39, 40]. In the $\pi^+\pi^-$ invariant mass, it can be seen that the wave-function amplitude distortions from the decay of the $a_1(1260)$ produced a significant impact on the $a_1(1260)\pi^-\pi^-\pi^+$ invariant mass distribution. This mainly comes in through the modification of

⁸The strong annihilation mixing will also impact the $\eta\eta$ and $\eta'\eta'$ wave-function amplitude distortions, potentially shifting it below the $\eta\eta$ and $\eta'\eta'$ productions threshold.

$\Gamma(s)$ in the propagator due to the wave-function amplification distortions, in contrast to the $f_0(1370)$ where the wave-function amplitude distortions directly impact the cross-section. The wave-function amplitude distortions from the decay of the $a_1(1260)$ also enhances the low mass scalar region through enhancements of the $f_0(1370)$ and an improved $a_1(1260)$ line-shape, providing a plausible alternative explanation to the low mass scalar hypothesis proposed in [50].

When extracting the distortion to the wave-function amplitude using the procedure in Section 2, it was assumed that the wave-function has propagated to r sufficiently large enough that it can be approximated by a plane wave. However, unlike the pseudo-scalar mesons, the vector meson, $\rho(770)$ and $K^*(892)$ have a relatively short life-time. More specifically, the flight length of the $K^*(892)$ meson is $c\tau\beta = \frac{c\beta}{\Gamma} \approx 5fm \times \beta$, while for the $\rho(770)$ meson is $c\tau\beta = \frac{c\beta}{\Gamma} \approx 1.3fm \times \beta$. These distances are comparable to the sizes of the outgoing mesons, $r_\pi = 0.659 \pm 0.004fm$ and $r_K = 0.56 \pm 0.031fm$ [9], and therefore the potentials. This means the wave-functions are still being modified by the inter-meson potentials when they decay and that the amplitude corrections do not fully describe the process. This is particularly important since, in Figure 5, it can be seen that the wave-function amplitude distortion in the S-wave channel at low energy in the decays of axial-vector mesons plays a significant role, in both the $a_1(1260)$ and $K_1(1270)$ line-shape. Moreover, from the decays of the $a_1(1260)$ and K_1 states, it can be seen that there is a non-negligible distortion to the $\rho(770)$ line shape when compared to the direct production mechanism, $\tau^- \rightarrow \rho^-(770)\nu_\tau$ and $\tau^- \rightarrow K^{*-}(892)\nu_\tau$. Since the residual QCD interaction between mesons is not typically taken into account in the experimental measurements, it may explain why the $\rho(770)$ meson and $K^*(892)$ decay widths depend on the production mechanism [9]. In the non-S-wave decay processes, it may be possible to probe the linear-confining potential and colour-Coulomb potential with multiple production mechanisms which would have different residual QCD potentials but with the same resonance shape.

5 Conclusion

Residual QCD inter-meson potentials are found to have a non-negligible impact on the vector and axial-vector meson production in addition to the well known wave-function enhancements in the scalar states which can be interpreted as meson-meson molecular states [1, 2, 3, 4, 5]. We presented an improved model of the $f_0(1370)$ by including the missing $f_0(1370) \rightarrow \gamma\gamma$ decay channel. The addition of inter-meson residual QCD potentials due to the colour hyper-fine spin-spin interaction has a significant impact on the spectrum. Only the $\pi\pi$ decay channel would show the double peak structure results from the dispersion relations. This could be investigated in decays of the $a_1(1260) \rightarrow \pi^- f_0(1370) (\rightarrow \pi\pi)$ or in two-photon production $\gamma\gamma \rightarrow f_0(1370) (\rightarrow \pi\pi)$. The ratio of $\pi\pi$ and KK

production in $f_0(1370)$ near 0.980GeV ($f_0(980)$) is a signature for these inter-meson residual QCD potentials [3]. There is already some supporting experimental evidence for the molecular description of the $f_0(500)$, $f_0(980)$ and $a_0(980)$ mesons [3, 4, 5]. The exact enhancement of $\pi\pi$ and KK production will depend on the quark composition predicted by the mixing of meson states, a consequence of the strong annihilation [4]. The residual inter-meson QCD potentials also have a non-negligible impact on the $a_1(1260)$ and K_1 state, particularly on the 3-body invariant mass distribution. For the $a_1(1260)$, this represents a substantial improvement in the agreement between the Flux-Tube Breaking Model predictions in [26] and the data [51].

Acknowledgement

I would like to thank Zbigniew Was for drawing my attention to the discrepancy in the low mass region which is not well understood. GCC Version 4.8.5 was used for compilation and the plots are generated using the external program GNUPlot [52].

References

- [1] J.D. Weinstein and N. Isgur. Do Multi-Quark Hadrons Exist? *Phys. Rev. Lett.*, 48:659, 1982. doi: 10.1103/PhysRevLett.48.659.
- [2] J.D. Weinstein and N. Isgur. The q q anti-q anti-q System in a Potential Model. *Phys. Rev. D*, 27:588, 1983. doi: 10.1103/PhysRevD.27.588.
- [3] T. Barnes, K. Dooley, and N. Isgur. Final-State Interactions and Anomalous Low-Energy $\pi\pi$ Production. *Phys. Lett. B*, 183: 210–214, 1987. doi: 10.1016/0370-2693(87)90440-0.
- [4] J.D. Weinstein and N. Isgur. KK Molecules. *Phys. Rev. D*, 41: 2236, 1990. doi: 10.1103/PhysRevD.41.2236.
- [5] N. Isgur, K. Maltman, J.D. Weinstein, and T. Barnes. A Potential Contribution to the $\Delta I=1/2$ Rule in $K \rightarrow \pi\pi$. *Phys. Rev. D*, 64:161, 1990. doi: 10.1103/PhysRevD.64.161.
- [6] T. Barnes. Two Photon Decays Support the (K anti-K) Molecular Picture of the $S^*(975)$. *Phys. Lett. B*, 165:434–440, 1985. doi: 10.1016/0370-26-93(85)91261-4.
- [7] P. O'Donnell, M. Frank, N. Isgur, and J.D. Weinstein. The Puzzle of the Iota: A Comment on the Decay. In *20th Rencontres de Moriond: QCD and Beyond*, pages 497–502, 1985.
- [8] J.D. Weinstein. Unraveling the Iota delta Mystery (How the delta is seen but is not there). In *Annual Meeting of the Division of Particle and Fields of the APS*, page 8, 1985.
- [9] P.A. Zyla et al. Review of Particle Physics. *Prog. Theor. and Exp. Phys.*, 2020(8), 2020. doi: 10.1093/ptep/ptaa104. URL https://pdg.lbl.gov/2020/hadronic-xsections/rpp2020-hadronicrpp_page1001.dat. 082C01.
- [10] J.A. Oller, E. Oset, and J.R. Pelaez. Meson-Meson Interactions in a Nonperturbative Chiral Approach. *Phys. Rev. D*, 59: 074001, 1999. doi: 10.1103/PhysRevD.59.074001.
- [11] J.R. Pelaez. Light Scalar as Tetraquarks or Two Meson States from Large N_c and Unitarized Chiral Perturbation Theory. *Mod. Phys. Lett. A*, 19(39):2879–2894, 2004. doi: 10.1142/s0217732304016160.
- [12] A. Dobado and J.R. Pelaez. Inverse Amplitude Method in Chiral Perturbation Theory. *Phys. Rev. D*, 56(5):3057–3073, 1997. doi: 10.1103/PhysRevD.56.3057.
- [13] J.A. Oller. Finite Width Effects in ϕ Radiative Decays. *Nucl. Phys. A*, 714(1-2):161–182, 2003. doi: 10.1016/S0375-9474(02)01360-X.
- [14] N. A. Törnqvist. Comparing the Broken $U3 \times U3$ Linear Sigma Model with Experiment. *Euro. Phys. J. C*, 11(2):359–363, 1999. doi: 10.1007/s100529900192.
- [15] M. Napsuciale and S. Rodriguez. A Chiral $q\bar{q}q\bar{q}$

- Nonet? *Phys. Lett. B*, 603(3-4):195–202, 2004. doi: 10.1016/j.physletb.2004.10.018.
- [16] M. Napsuciale and S. Rodriguez. A Chiral Model for $\bar{q}q$ and $q\bar{q}q$ Mesons. *Phys. Rev. D*, 70(9):094043, 2004. doi: 10.1103/PhysRevD.70.094043.
- [17] M. Ishida. Possible Classification of the Chiral Scalar σ -Nonet. *Prog. of Theor. Phys.*, 101(3):661–669, 1999. doi: 10.1143/ptp.101.661.
- [18] M.D. Scadron. Scalar σ Meson via Chiral and Crossing Dynamics. *Euro. Phys. J. C*, 6(1):141–145, 1999. doi: 10.1007/s100520050327.
- [19] A.H. Fariborz, J. Schechter, S. Zarepour, and S.M. Zebarjad. Chiral Nonet Mixing in $\eta' \rightarrow \eta\pi\pi$ Decays. *Phys. Rev. D*, 90:033009, 2014. doi: 10.1103/PhysRevD.90.033009.
- [20] D. Black, A.H. Fariborz, F. Sannino, and J. Schechter. Perturbative Light Scalar Nonet. *Phys. Rev. D*, 59(7). doi: 10.1103/PhysRevD.59.074026.
- [21] M. Gell-Mann and M. Lévy. The axial vector current in β decays. *Il Nuovo Cimento*, 16:705–726, 1960. doi: 10.1007/BF02859738.
- [22] T. H. R. Skyrme. A non-linear field theory. *Proc. Roy. Soc. Lond. A*, 260:127–138. doi: 10.1098/rspa.1961.0018.
- [23] T. H. R. Skyrme. A Unified Field Theory of Mesons and Baryons. *Nucl. Phys.*, 31:556–569, 1962. doi: 10.1016/0029-5582(62)90775-7.
- [24] J. M. Speight. A Simple Mass Splitting Mechanism in the Skyrme Model. *Phys. Lett. B*, 781:455–458, 2018. doi: 10.1016/j.physletb.2018.04.026.
- [25] Y. Nambu and G. Jona-Lasinio. Dynamical Model of Elementary Particles Based on an Analogy with Superconductivity. I*. *Phys. Rev.*, 122:345–358, 1961. doi: 10.1103/PhysRev.122.345.
- [26] I. M. Nugent. **eeMC**: Simulation of $e^+e^- \rightarrow \mu^+\mu^-(\gamma)$ and $e^+e^- \rightarrow \tau^+\tau^-(\gamma)$ Events. 2022. arXiv: 2202.02318 [hep-ph].
- [27] Richard Kokoski and Nathan Isgur. Meson Decays by Flux Tube Breaking. *Phys. Rev. D*, 35:907, 1987. doi: 10.1103/PhysRevD.35.907.
- [28] N. Isgur and J.E. Paton. A Flux Tube Model for Hadrons. *Phys. Lett. B*, 124:247–251, 1983. doi: 10.1016/0370-2693(83)91445-4.
- [29] N. Isgur and J.E. Paton. A Flux Tube Model for Hadrons in QCD. *Phys Rev D.*, 31:2910, 1984. doi: 10.1103/PhysRevD.31.2910.
- [30] Nathan Isgur, Colin Morningstar, and Cathy Reader. The a_1 in τ Decay. *Phys. Rev. D*, 39:1357, 1989. doi: 10.1103/PhysRevD.39.1357.
- [31] M. Abramowitz and I. A. Stegun. *Handbook of Mathematic Functions*. Dover Publications Inc., New York, USA, 1964. ISBN 0-486-61272-4.
- [32] Wen Shen. *An Introduction to Numerical Computation*. World Scientific, 2016. ISBN 978-981-4730-06-08.
- [33] R.L. Liboff. *Introductory Quantum Mechanics 3rd Ed*. Addison-Wesely Publishing Company, Inc., 1997. ISBN 0-201-87879.
- [34] T. Barnes, N. Black, D.J. Dean, and E.S. Swanson. BB Inter-meson Potentials in the Quark Model. *Phys. Rev. D*, 602. doi: 10.1103/PhysRevC.60.045202.
- [35] S. Godfrey and Nathan Isgur. Mesons in a Relativized Quark Model with Chromodynamics. *Phys. Rev. D*, 32:189–231, 1985. doi: 10.1103/PhysRevD.32.189.
- [36] G.B. Arfken and H.J. Weber. *Mathematical Methods for Physicists 5th Ed*. Harcourt/Academic Press, London, UK, 2001. ISBN 0-12-059825-6.
- [37] D. Scora and N. Isgur. Semileptonic Meson Decays in the Quark Model: An Update. *Phys. Rev. D*, 52:2783–2812, 1995. doi: 10.1103/PhysRevD.52.2783.
- [38] Mahiko Suzuki. Strange Axial-Vector Meson. *Phys. Rev. D*, 42:1252–1255, 1993. doi: 10.1103/PhysRevD.47.1252.
- [39] H. G. Bludell, S. Godfrey, and B. Phelps. Properties of the Strange Axial Meson in the Relativized Quark Model. *Phys. Rev. D*, 53:3712–3722, 1996. doi: 10.1103/PhysRevD.53.3712.
- [40] D.M. Asner et al. Resonance Structure of $\tau^- \rightarrow K^- \pi^+ \pi^- \nu_\tau$ Decays. *Phys. Rev. D*, 62:072006, 2000. doi: 10.1103/PhysRevD.62.072006.
- [41] H. Saazdjian. The Interplay between Compact and Molecular Structures in Tetraquarks. *Symmetry*, 14(3):515, 2022. doi: 10.3390/sym14030515.
- [42] J.D. Walecka. *Introduction to Modern Physics Theoretical Foundations*. World Scientific, Singapore, 2008. ISBN 978-9812812247.
- [43] R.D. Woods and D.S. Saxon. Diffusion Surface Optical Model for Nucleon-Nuclei Scattering. *Phys. Rev. D*, 95:577, 1954. doi: 10.1103/PhysRevD.95.577.
- [44] L. Bergstrom, G. Hulth, and H. Snellman. Relativistic Calculation of the Two Photon Coupling of Scalar and Tensor Mesons. *Z. Phys. C*, 16:263, 1983. doi: 10.1007/BF01571614.
- [45] J.R. Pelaez. From Controversy to Precision on the σ Meson: A Review on the Status of the Non-ordinary $f_0(500)$ Resonance. *Phys. Rept.*, 658:1, 2016. doi: 10.1016/j.physrep.2016.09.001.
- [46] B. Moussallam. Coupling of Light $I=0$ Scalar Meson to Simple Operators in the Complex Plane. *Eur. Phys. J. C.*, 71:1814, 2011. doi: 10.1140/epjc/s10052-011-1814-z.
- [47] Y. Mao, X. Wang, O. Zhang, H.Q. Zheng, and Z.Y. Zhou. A dispersive Analysis on the $f_0(600)$ and $f_0(980)$ Resonance in the $\gamma\gamma \rightarrow \pi^+\pi^-, \pi^0\pi^0$ Process. *Phys. Rev. D*, 79:116008, 2009. doi: 10.1103/PhysRevD.79.116008.
- [48] G.J. Gounaris and J.J. Sakurai. Finite Width Corrections to the Vector Meson Dominance Prediction for $\rho \rightarrow e^+e^-$. *Phys. Rev. Lett.*, 21:244–247, 1968. doi: 10.1103/PhysRevLett.21.244.
- [49] J.P. Lees et al. Precise Measurement of the $e^+e^- \rightarrow \pi^+\pi^-(\gamma)$ Cross Section with the Initial-State Radiation Method at BABAR. *Phys. Rev. D*, 86:032013, 2012. doi: 10.1103/PhysRevD.86.032013.
- [50] I.M. Nugent, T. Przedziński, P. Roig, O. Shekhovtsova, and Z. Wąs. Resonance Chiral Lagrangian Currents and Experimental Data for $\tau^- \rightarrow \pi^- \pi^- \pi^+ \nu_\tau$. *Phys. Rev. D*, 88:093012, 2013. doi: 10.1103/PhysRevD.88.093012.
- [51] Bernard Aubert et al. Exclusive Branching Fraction Measurements of Semileptonic τ Decays into Three Charged Hadrons, $\tau^- \rightarrow \phi \pi^- \nu_\tau$ and $\tau^- \rightarrow \phi K^- \nu_\tau$. *Phys. Rev. Lett.*, 100:011801, 2008. doi: 10.1103/PhysRevLett.100.011801.
- [52] Thomas Williams, Colin Kelley, et al. Gnuplot 4.2: An Interactive Plotting Program. <http://gnuplot.sourceforge.net/>, 2007.
- [53] J. H. Kühn and A. Santamaria. Tau Decays to Pions. *Z. Phys. C*, 48:445–452, 1990. doi: 10.1007/BF01572024.
- [54] Markus Finkemeier and Erwin Mirkes. Tau Decays into Kaons. *Z. Phys. C*, 69:243–252, 1996.
- [55] T. Abe et al. Belle-II Technical Design Report, 2010.
- [56] E. Kou and other. The Belle II Physics Book. *Progress of Theoretical and Experimental Physics*, 2019(12), 2019. doi: 10.1093/ptep/ptz106.
- [57] D. M. Asner et al. Hadronic Structure in the Decay $\tau^- \rightarrow \nu_\tau \pi^- \pi^0 \pi^0$ and the Sign of the Tau Neutrino Helicity. *Phys. Rev. D*, 61:012002, Dec 1999. doi: 10.1103/PhysRevD.61.012002.
- [58] I.M. Nugent. Invariant Mass Spectra of $\tau^- \rightarrow h^- h^- h^+ \nu_\tau$ Decays. *Nucl. Phys. B - Proc. Suppl.*, 253-255:38–41, 2014. doi: 10.1016/j.nuclphysbps.2014.09.010.

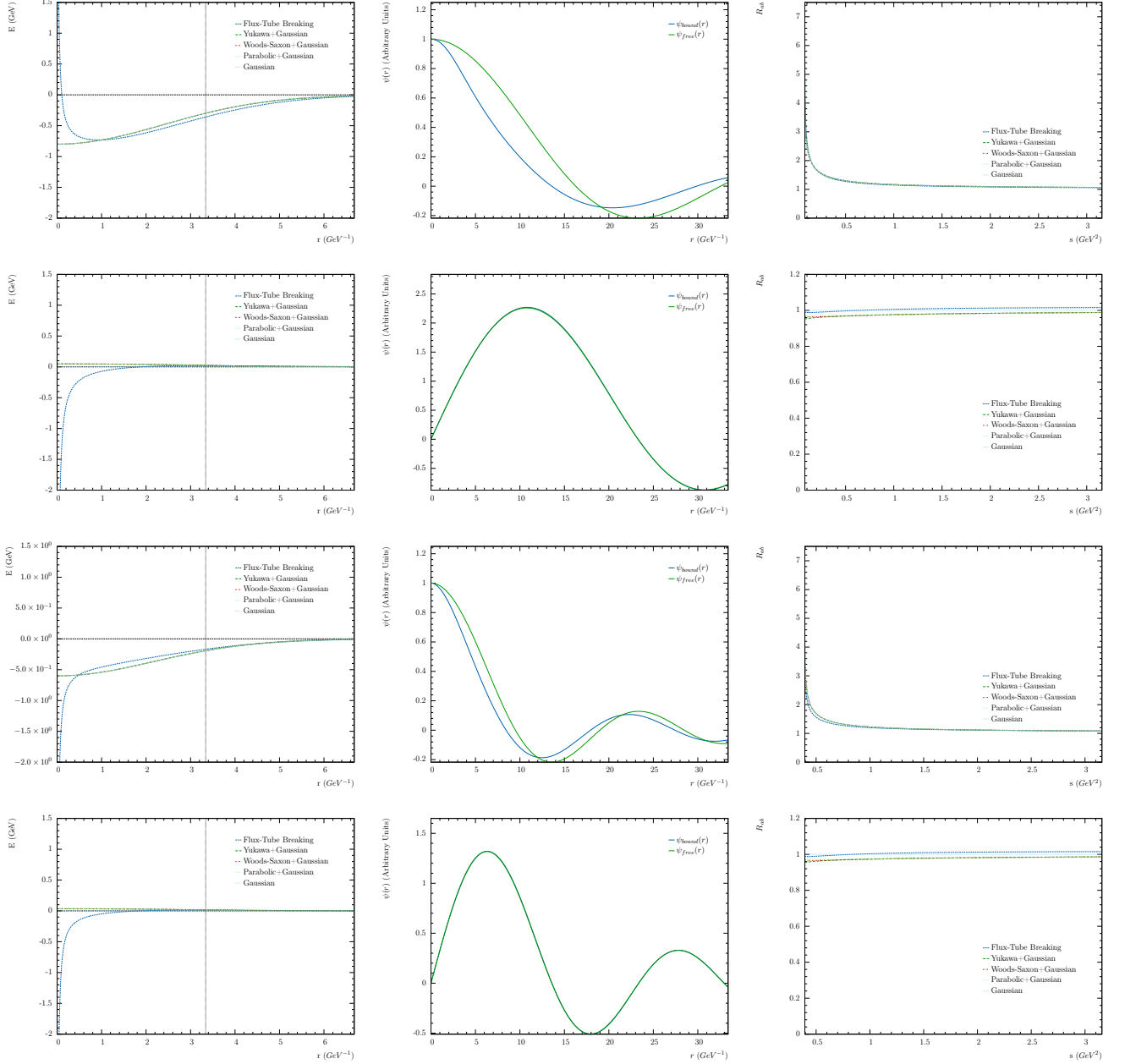


Figure 1: The effective potentials including angular momentum (left), wave-function solutions for the Flux-Tube Breaking Model with $s=1.25 \times s_{\text{thres}}$ (middle) and the wave-function distortion factor $S_{h_1 h_2}^2$ (right) for the effective potential models presented in Table 1 for the $\pi^+ \pi^-$ [$l=0$] (top), [$l=1$] (upper-middle), $K^- \pi^0$ [$l=0$] (lower-middle), [$l=1$] (bottom) Final-States. The angular momentum potential $l(l+1)/(2\mu r^2)$ is not included in the figures, but has been included in the calculation.

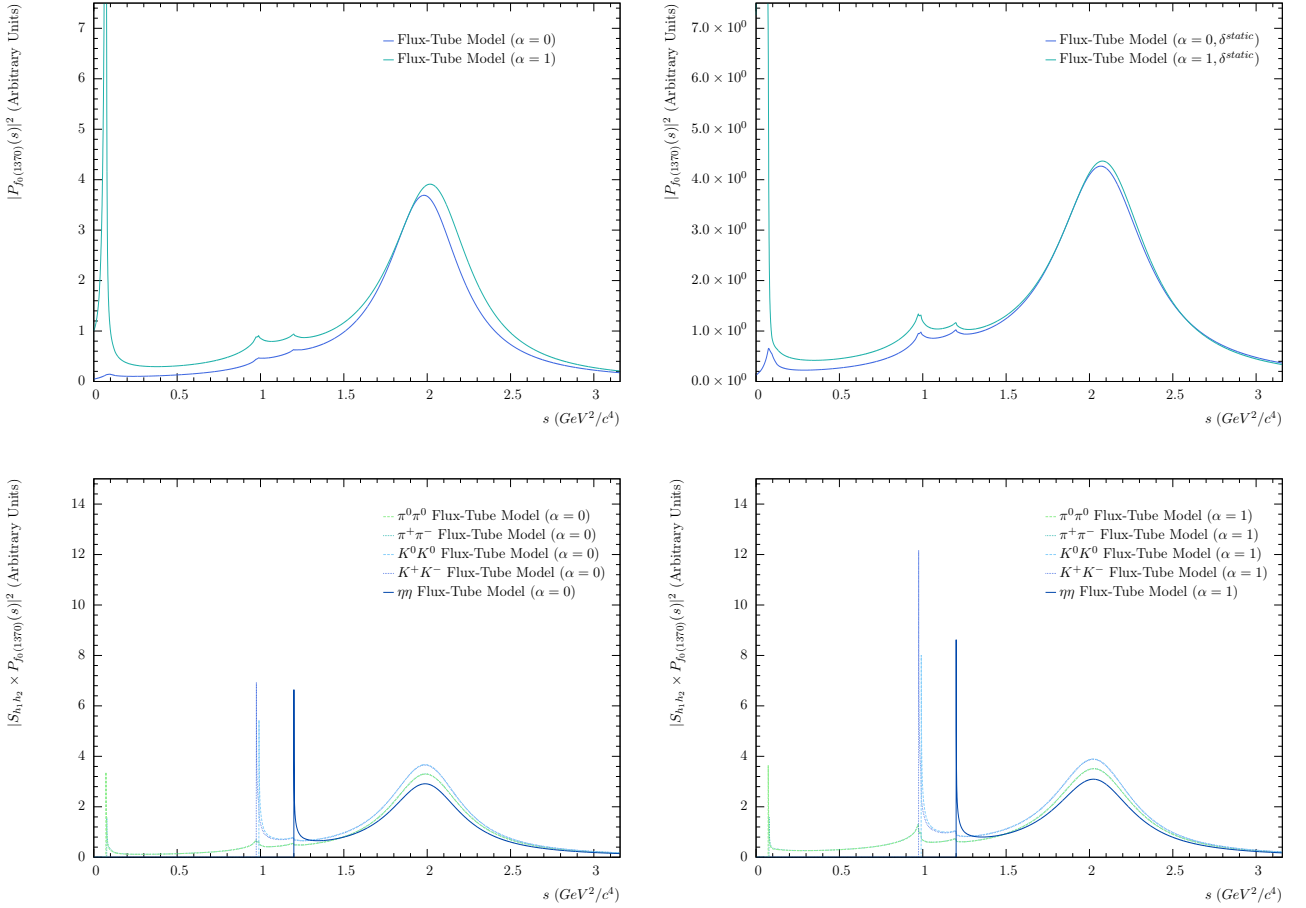


Figure 2: A comparison of the $f_0(1370)$ propagator line shape with the $f_0(1370) \rightarrow \gamma\gamma$ channel included (top-left), with the $f_0(1370) \rightarrow \gamma\gamma$ channel included using the static limit $[\delta^{static}]$ (top-right) $f_0(1370)$ propagator with the wave-function amplitude distortions for $\alpha=0$ (bottom-left) and $\alpha=1$ (bottom-right). The $f_0(1370)$ propagator is amplified through the dispersion relations near the $\pi^0\pi^0$ threshold where the only decay channel is $f_0(1370) \rightarrow \gamma\gamma$. For $\alpha=1$ this enhancement does not appear physical. Depending on the mixing in the strong annihilation process, the residual QCD amplification from the wave-function amplitude distortion may not produce an amplification in the $\eta\eta$ channel at threshold, but instead would contribute to the amplification of the $K^+K^-/K^0\bar{K}^0$ channels [4].

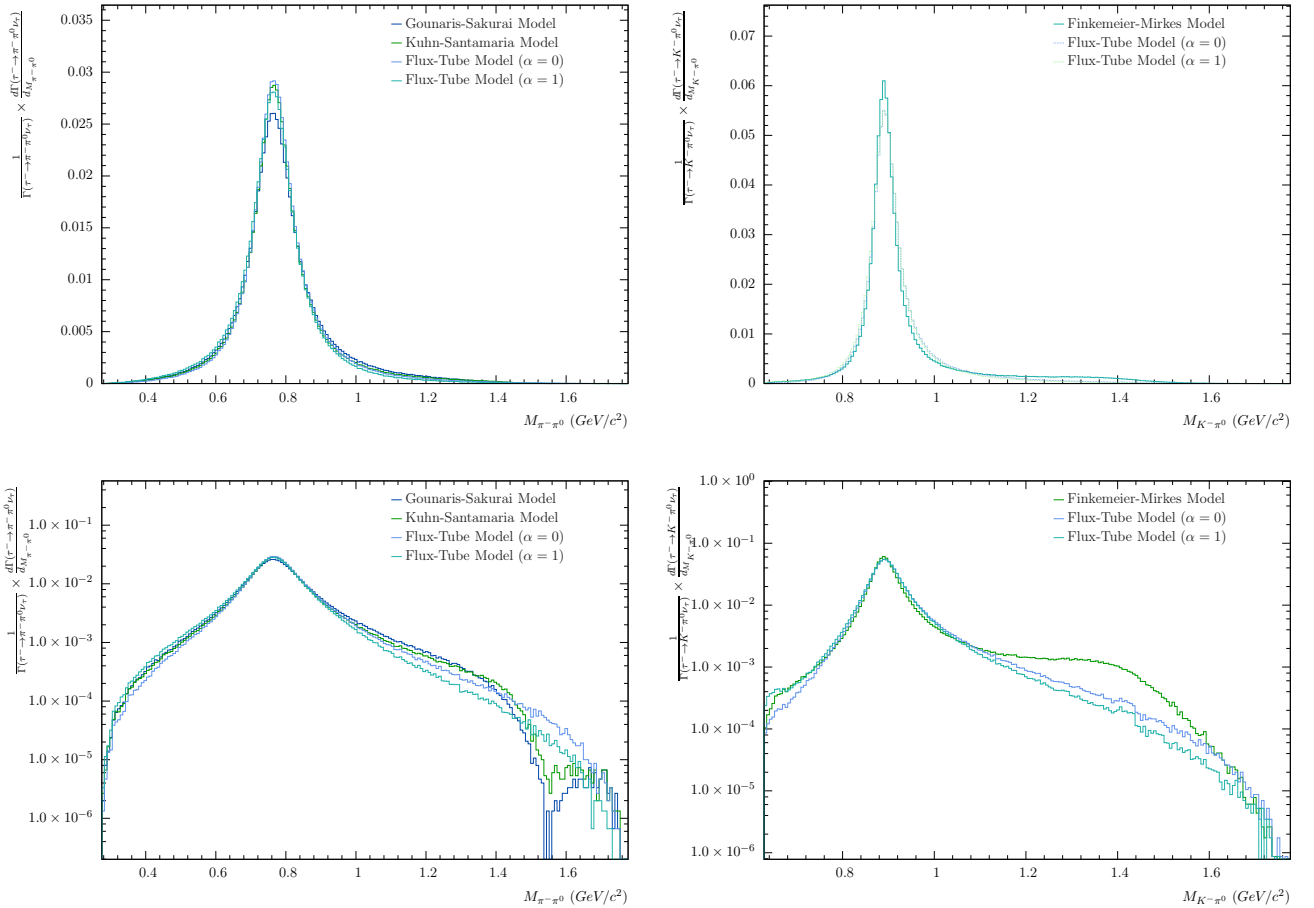


Figure 3: The differential invariant mass spectra for $\tau^- \rightarrow \rho(770) \rightarrow \pi^+ \pi^0 \nu_\tau$ in linear (top-left) and log (bottom-left) scale, $\tau^- \rightarrow K^*(892)/K_0^*(1430) \rightarrow K^+ \pi^- \nu_\tau$ in linear (top-right) and log (bottom-right) scale with the molecular wavefunction distortion factor $S_{h_1 h_2}^2$. In the $\tau^- \rightarrow \rho(770) \rightarrow \pi^+ \pi^0 \nu_\tau$, the Gounaris-Sakurai Model [48] using the parameterization extracted from $e^+ e^- \rightarrow \pi^+ \pi^- \gamma$ data [49], and the Kühn-Santamaria Model [53] with improved parameterization [49] are super-imposed to illustrate the improvement in the agreement with other models, while the Finkemeier-Mirkes Model [54] is super-imposed on the $\tau^- \rightarrow K^*(892)/K_0^*(1430) \rightarrow K^+ \pi^- \nu_\tau$ channel. The most significant difference between the Flux-Tube Breaking Model compared to the Gounaris-Sakurai Model [48] and ChRL Models is due to the missing higher mass resonance.

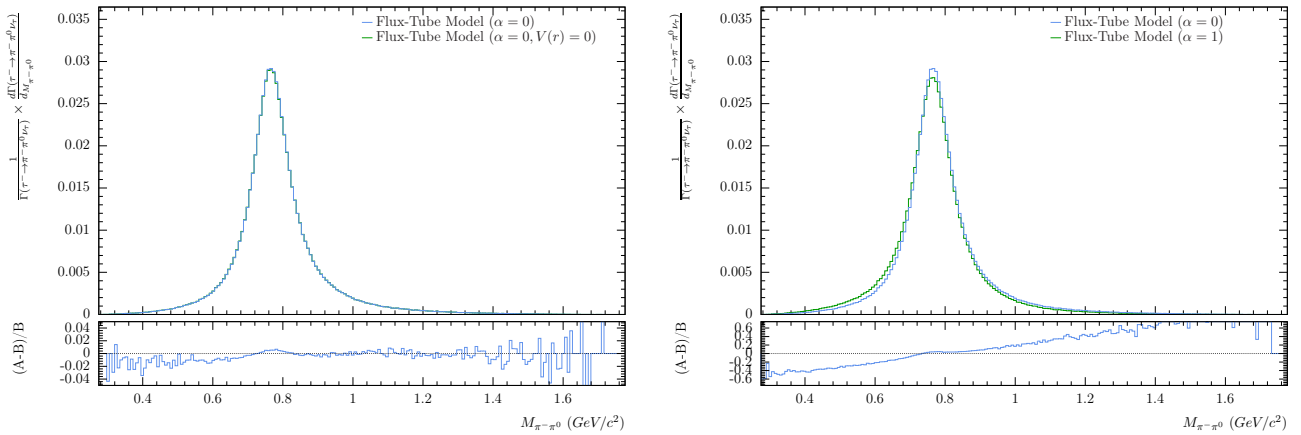


Figure 4: A comparison of the differential invariant mass spectra for $\tau^- \rightarrow \rho(770) \rightarrow \pi^+ \pi^0 \nu_\tau$ in the Flux-Tube Breaking Model with and without the wave-function amplitude distortion (left) and with $\alpha=0$ and $\alpha=1$ (right) simulated for 1×10^6 events. The lower plot represents the relative difference between the distributions. At BELLE-II, the expected statistics after events selection for the $\tau^- \rightarrow \rho(770) \rightarrow \pi^+ \pi^0 \nu_\tau$ will be more than $100\times$ greater than presented here [55, 56].

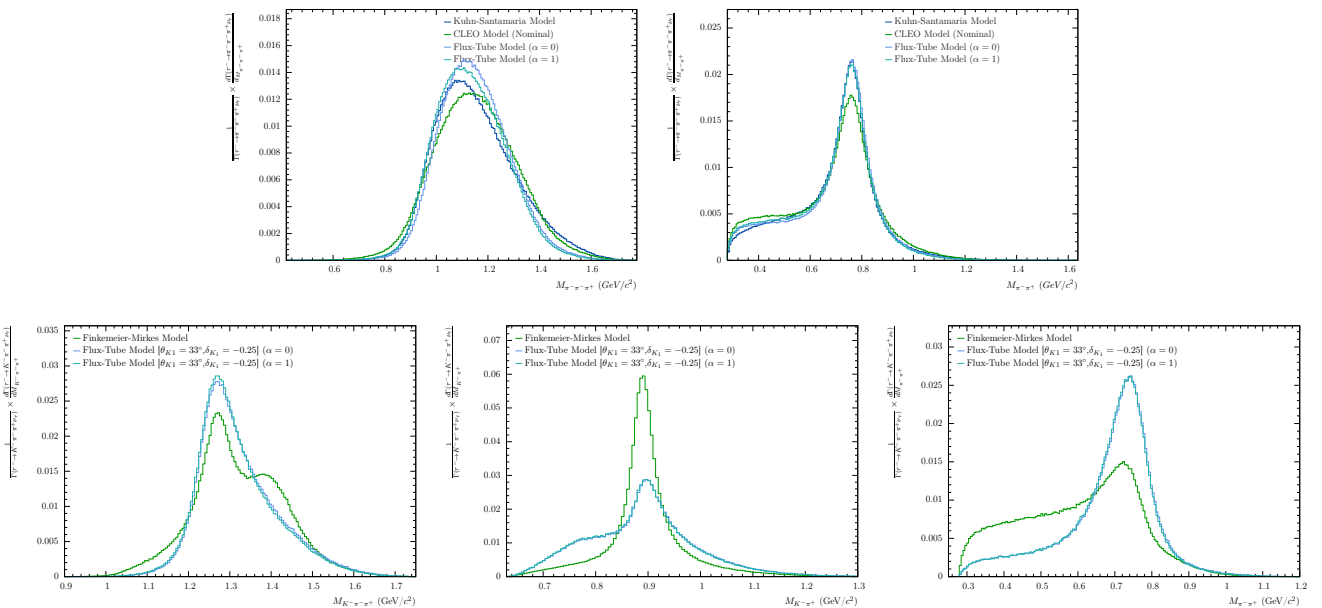


Figure 5: The differential invariant mass spectra $\pi^- \pi^- \pi^+$ (top-left) and $\pi^- \pi^+$ (top-right) for the $\tau^- \rightarrow a_1(1260) \rightarrow \pi^- \pi^- \pi^+ \nu_\tau$, and $K^- \pi^- \pi^+$ (bottom-left), $K^- \pi^+$ (bottom-middle) and $\pi^- \pi^+$ (bottom-right) $\tau^- \rightarrow K_1(1270/1400) \rightarrow K^- \pi^- \pi^+ \nu_\tau$ with the molecular wave-function distortion factor $S_{h_1 h_2}^2$. The Kühn-Santamaria Model [53] and CLEO Model [57] are super-imposed to illustrate the improvement in the agreement of the Flux Tube Breaking Model when compared to the other models for the $\tau^- \rightarrow a_1(1260) \rightarrow \pi^- \pi^- \pi^+ \nu_\tau$ channel. When compared to the experimental data [51, 58], this improvement in the Flux-Tube Breaking Model is reflected through a tunable increase in the low mass $\pi^+ \pi^+$ invariant mass spectra and narrower $a_1(1260)$ line-shape which is more consistent with the data [51, 58]. For the $\tau^- \rightarrow K_1(1270/1400) \rightarrow K^- \pi^- \pi^+ \nu_\tau$ channel, the Finkemeier-Mirkes Model [54] is super-imposed on the $\tau^- \rightarrow K_1(1270/1400) \rightarrow K^- \pi^- \pi^+ \nu_\tau$ channel. The disagreement in the $\pi^+ \pi^-$ and $K^- \pi^+$ spectra in the K_1 invariant mass distributions, when compared to [51, 58], indicates that the value $\theta_{K_1} = 33^\circ$ is inconsistent with the experimental data.

Table 1: The definition of the residual QCD potentials. The parameters are defined in Table 2.

Potential	Equation
Spherical-Gaussian [3]	$V(r)=V_0 e^{-\frac{r^2}{2r_0^2}} \quad (11)$
Shell Model (Woods-Saxon) [42, 43]	$V(r)=V_0 \left(\frac{1 + e^{-\frac{a_0}{s_0}}}{1 + e^{-\frac{r-a_0}{s_0}}} \right) \quad (12)$
Shell Model (Parabolic) [42]	$V(r)=\begin{cases} 0, & r > a_0\sqrt{2} \\ V_0 \left(1 - \left(\frac{r}{\sqrt{2}a_0} \right)^2 \right), & \text{if } r < a_0\sqrt{2} \end{cases} \quad (13)$
Parabolic-Yukawa Model	$V(r)=\begin{cases} V_0 \left(\frac{a_0}{r} \right) e^{-\frac{r}{a_0}}, & r > a_0 \\ V_0 \left(\frac{1}{2} \right) \left(1 + \left(1 - \left(\frac{r}{a_0} \right)^2 \right) \right), & \text{if } r < a_0 \end{cases} \quad (14)$

Table 2: The model parameters for the residual QCD potentials. The charge radius of the pion (r_π) and kaon (r_K) are from [9]. The normalization of the strength of the residual QCD potentials, V_0 , are based on [3].

Decay	V_0 (GeV)	a_0	$s_{thickness}$
$\pi^{0,\pm}, \rho^{0,\pm}, f_0(1370)$	0.4	r_π	0.27
$K^{0,\pm}, K^{*(0,\pm)}(892), K_0^*(1430)$	0.2	r_K	0.27
$\eta, \eta'(958)$	0.1	$r_K/\sqrt{2}$	0.27